Acta Pharmaceutica Sinica B 2019;9(3):626–638

Chinese Pharmaceutical Association
Institute of Materia Medica, Chinese Academy of Medical Sciences

Acta Pharmaceutica Sinica B

www.elsevier.com/locate/apsb
www.sciencedirect.com

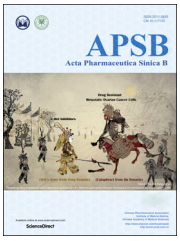

ORIGINAL ARTICLE

Combinatorial mutation on the β-glycosidase specific to 7-β-xylosyltaxanes and increasing the mutated enzyme production by engineering the recombinant yeast

Jing-Jing Chen, Xiao Liang, Fen Wang, Yan-Hua Wen, Tian-Jiao Chen, Wan-Cang Liu, Ting Gong, Jin-Ling Yang, Ping Zhu*

State Key Laboratory of Bioactive Substance and Function of Natural Medicines & NHC Key Laboratory of Biosynthesis of Natural Products, Institute of Materia Medica, Chinese Academy of Medical Sciences & Peking Union Medical College, Beijing 100050, China

Received 5 September 2018; received in revised form 8 November 2018; accepted 18 November 2018

KEY WORDS

β-Glycosidases;
Combinatorial mutation;
Improved catalytic property;
Molecular docking;
Engineered yeast;
Taxol

Abstract Taxol is a "blockbuster" antitumor drug produced by *Taxus* species with extremely low amount, while its analogue 7-β-xylosyl-10-deacetyltaxol is generally much higher in the plants. Both the fungal enzymes LXYL-P1−1 and LXYL-P1−2 can convert 7-β-xylosyl-10-deacetyltaxol into 10-deacetyltaxol for Taxol semi-synthesis. Of them, LXYL-P1−2 is twice more active than LXYL-P1−1, but there are only 11 significantly different amino acids in terms of the polarity and acidic-basic properties between them. In this study, single and multiple site-directed mutations at the 11 sites from LXYL-P1−1 to LXYL-P1−2 were performed to define the amino acids with upward bias in activities and to acquire variants with improved catalytic properties. Among all the 17 mutants, E12 (A72T/V91S) was the most active and even displayed 2.8- and 3-fold higher than LXYL-P1−2 on β-xylosidase and β-glucosidase activities. The possible mechanism for such improvement was proposed by homology modeling and molecular docking between E12 and 7-β-xylosyl-10-deacetyltaxol. The recombinant yeast GS115-P1E12-7 was constructed by introducing variant *E12*, the molecular chaperone gene *pdi* and the bacterial hemoglobin gene *vhb*. This engineered yeast rendered 4 times higher biomass enzyme activity than GS115-3.5K-P1−2 that had been used for demo-scale fermentation. Thus, GS115-P1E12-7 becomes a promising candidate to replace GS115-3.5K-P1−2 for industrial purpose.

*Corresponding author. Tel.: 8610-63165197; fax: 8610-63017757.
E-mail address: zhuping@imm.ac.cn (Ping Zhu).

Peer review under responsibility of Institute of Materia Medica, Chinese Academy of Medical Sciences and Chinese Pharmaceutical Association.

https://doi.org/10.1016/j.apsb.2018.11.003

1. Introduction

Glycoside hydrolases (GHs, EC 3.2.1), also known as glycosidases, are enzymes that can hydrolyze the glycosidic bonds in glycoconjugates[1–4]. GHs can be categorized into over 100 families based on the amino acid sequences of different species. Of them, β-xylosidases can mainly be classified into the 3, 30, 39, 43, 52 and 54 GH families[5]. β-Xylosidases, the exogenous glycosidases that are widely distributed in nature, have been isolated from bacteria, actinomyces, fungi and some higher plants[6,7]. They can not only catalyze the hydrolysis of hemicellulosic xylans and remove the successive D-xylose residues from the non-reducing termini, but can also hydrolyze the glycosidic bonds between the xylose residue and aglycone of β-xylosyl-terpenes or steroids[5]. Taxol (generic name: paclitaxel) refers to a diterpenoid compound with definite anti-cancer activity[8–10]. At present, Taxol from nursery cultivated *Taxus* species accounts for one of the main sources for clinical supply. However, its natural content is extremely low, which ranges from 0 to 0.069%, and the highest content is found in the bark. In comparison, the content of its analogue 7-β-xylosyl-10-deacetyltaxol (XDT) is generally much higher than that of Taxol. Typically, if the xylosyl group of XDT is removed, the corresponding 10-deacetyltaxol (DT) can be converted into Taxol by acetylation at the C10 position. However, such analogue is generally discarded during Taxol extraction, leading to both resource waste and potential environmental pollution[11]. In our previous study, two variants, LXYL-P1−1 and LXYL-P1−2 with dual GH3 β-xylosidase/β-glucosidase activities, were cloned from *Lentinula edodes* (strain M95.33) and characterized. Most importantly, such enzymes can specifically remove the xylosyl group from XDT to produce DT for the semi-synthesis of Taxol (Scheme 1)[12,13].

Particularly, the activity of LXYL-P1−2 is twice higher than that of LXYL-P1−1. However, sequence analysis shows that both open reading frames (ORFs) have encoded 803 amino acids with over 97% sequence identity as well as 21 different amino acids. Moreover, all the 21 different amino acids are distributed in the first 386 positions of the two polypeptides[12]. Typically, 11 of these 21 different amino acids have exhibited significant differences in terms of their polarity and acidic-basic properties (Fig. 1). For instance, the positions of 3, 69, 192, 310, 318, 322, 327 and 334 are occupied by hydrophilic polar or acidic amino acids in LXYL-P1−1, while the corresponding sites in LXYL-P1−2 are taken up by hydrophobic non-polar or basic amino acids. On the contrary, amino acids in the positions 72, 91 and 368 are hydrophobic and non-polar in LXYL-P1−1, whereas those are hydrophilic polar amino acids in LXYL-P1−2 (Fig. 1). Therefore, some of these amino acids may affect the enzyme activity of both variants, although they are not involved in the substrate binding and catalytic sites. Specifically, the site-directed mutations of these amino acids from the low-active LXYL-P1−1 to the high-active LXYL-P1−2 can not only contribute to defining the amino acids with upward bias in activity, but can also make for obtaining the β-glycosidase variants with higher activities.

Pichia pastoris, the methylotrophic yeast, has been frequently used for the heterologous expression of a variety of industrially relevant biocatalysts and pharmaceutical proteins[14–16]. As an aerobic microorganism, *P. pastoris* requires continuous oxygen supply and efficient utilization for the expression of recombinant proteins, which is particularly true at the fermentation stage of *P. pastoris* with high cell density[17]. *Vitreoscilla* hemoglobin (VHB, coding gene: *vhb*) is produced by the gram-negative bacterium *Vitreoscilla*[18–22]. Wu et al.[23] reported that, the intracellular co-expression of *vhb* regulated by methanol-inducible promoter contributed to cell growth and β-galactosidase production in *P. pastoris*. In addition, Chen et al.[24] also suggested that, the co-expression of *vhb* could promote cell growth and SAM production, which was achieved through enhancing the ATP synthetic rate in the recombinant *P. pastoris*. Therefore, the heterologous expression of *vhb* may alleviate oxygen limitation at the later fermentation stage, thus facilitating cell density and protein production. Protein disulfide isomerase (PDI), which belongs to the molecular chaperone, participates in protein folding as well as assembly and contributes to the rearrangement of incorrect disulfide pairings[25,26]. Typically, the initial eukaryotic transcription process is sophisticated and is achieved under the assistance of many protein factors. UPC (sterol uptake control protein), a zinc finger transcription factor, regulates the ergosterol homeostasis through binding to the promoter region of eukaryotic gene with *cis*-acting elements[27]. UPC exerts no direct regulatory action on the heterologous expression of protein; nonetheless, it may affect protein production through interacting with other unknown target proteins. Therefore, the co-expression of the above factors with β-glycosidase gene may up-regulate the enzyme expression level. The β-glycosidases LXYL-P1−1 and LXYL-P1−2 have been successfully expressed in *P. pastoris*, and the recombinant yeast GS115-3.5K-P1−2 can be used as a biocatalyst to convert XDT into DT for the semi-synthesis of Taxol[12]. On this account, it is of practical significance to further enhance the biomass activity to reduce the costs of bioconversion.

In this study, the 11 aforementioned amino acids were changed from LXYL-P1−1 to LXYL-P1−2 by single and multiple site-directed mutations, so as to identify the key amino acids with upward bias in enzyme activity and to obtain variants with improved catalytic properties. Besides, genes encoding PDI (*P. pastoris* origin), VHB (*Vitreoscilla* origin) and UPC (*S. cereviase* origin) that were driven by inducible or constitutive promoters were introduced into the recombinant *Pichia pastoris* that expressed the mutated highly-active enzyme. Subsequently, the effects of these factors on the biomass activity were explored. Finally, the recombinant strains with apparently improved biomass activities could be obtained.

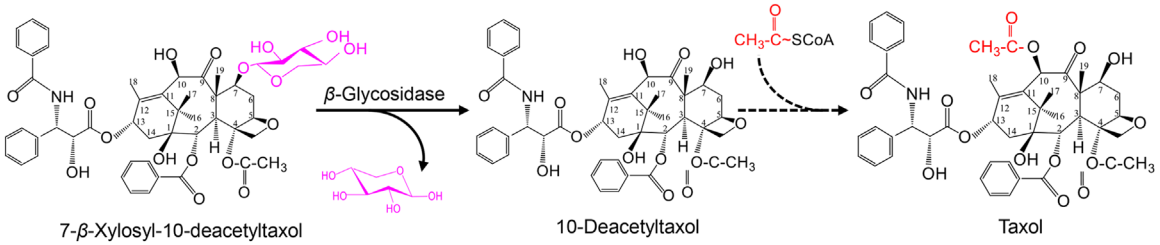

Scheme 1 Bioconversion of 7-β-xylosyl-10-deacetyltaxol to 10-deacetyltaxol for the semi-synthesis of Taxol.

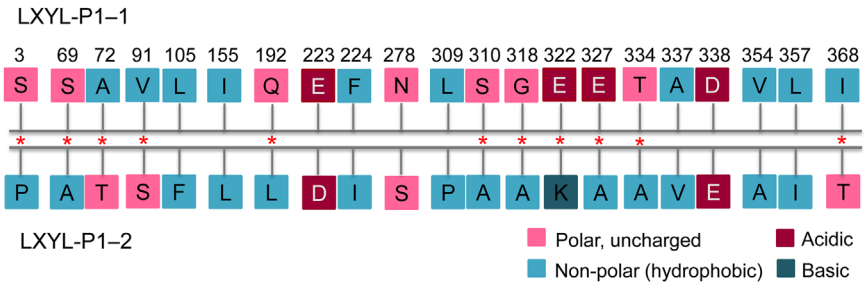

Figure 1 Polarity and acidic-basic properties of the 21 differential amino acids between LXYL-P1−1 and LXYL-P1−2. The amino acids with different polarity and acidic–basic properties are indicated in red asterisk.

2. Materials and methods

2.1. *Plasmids and strains*

All strains and plasmids used in this study are listed in Table 1 [12]. *Pichia pastoris* GS115 strain and plasmids (pPIC3.5 K, pPICZA, and pPIC6A) were purchased from Invitrogen. The recombinant plasmids pPIC3.5K-LXYL-P1−1 and pPIC3.5K-LXYL-P1−2 were previously constructed in our laboratory[11]. *Pichia pastoris* GS115-3.5K-P1−1 and GS115-3.5K-P1−2 were constructed by transforming the host strain *P. Pastoris* GS115 (Mut^+) with the plasmids pPIC3.5K-LXYL-P1−1 and pPIC3.5K-LXYL-P1−2, and preserved at −80 °C prior to use[12].

2.2. *Single and multiple site-directed mutagenesis of LXYL-P1−1*

The primers with single or multiple site-directed mutations are listed in Supporting Information Table S1. The single site-directed mutations in E1–E11 were conducted through whole-plasmid amplification PCR. Meanwhile, the expression plasmid pPIC3.5K-LXYL-P1−1, which harbored the glycoside hydrolase gene *Lxyl-p1−1*, was used as a template in the PCR reactions. PCR was performed with Phusion DNA polymerase (NEB, Ipswitch, MA, USA) using the following pairs of primers: S3P-F1/S3P-R1, S69A-F2/S69A-R2, A72T-F3/A72T-R3, V91S-F4/V91S-R4, Q192L-F5/Q192L-R5, S310A-F6/S310A-R6, G318A-F7/G318A-R7, E322K-F8/E322K-R8, E327A-F9/E327A-R9, T334A-F10/T334A-R10 and I368T-F11/I368T-R11, respectively. The PCR conditions for amplification consisted of 98 °C for 30 s, 30 cycles of 10 s at 98 °C, 30 s at 52–72 °C (each cycle increased 0.7 °C), 6 min at 72 °C, and a final 10 min extension at 72 °C. The PCR products were purified and digested by Dpn I at 37 °C for 3 h and then transformed into DMT competent cells (Transgen, Beijing, China). After the sequences were confirmed, the corresponding vectors were referred as pPIC3.5K-E1–E11.

Additionally, the multiple site-directed mutations of LXYL-P1−1 were performed using the PCR-based overlap extension method[28,29]. To construct the double mutant *E12*, the two individual fragments were amplified by Phusion DNA polymerase using primers P1−1-F/V91S-R and V91S-F/P1−1-R, respectively, with the plasmid pPIC3.5K-E3 being used as a template. Similarly, the PCR conditions for amplification consisted of 98 °C for 30 s, 30 cycles of 10 s at 98 °C, 30 s at 60 °C, 1 min at 72 °C, and a final 10 min extension at 72 °C. The PCR products were separated by gel electrophoresis and were purified using a gel extraction kit (Transgen, Beijing, China). Later, the overlap extension was performed by mixing 100 ng of the two fragments in equimolar amounts with Phusion PCR buffer, dNTPs, and Phusion polymerase in a total volume of 25 μL. The PCR conditions for amplification were 98 °C for 30 s, 15 cycles of 10 s at 98 °C, 30 s at 60 °C, 72 °C for 30 s/kb, followed a 10 min incubation at 72 °C. Then, 2 μL of the unpurified PCR product was further used as a template for the second round PCR. Additionally, P1−1-F and P1−1-R, Phusion PCR buffer, dNTPs, and Phusion polymerase were added into the PCR mixture in a final volume of 50 μL. The amplification was performed identically to the PCR reaction of the individual fragments. The fusion PCR products were separated by gel electrophoresis and purified using a gel purification kit, as described above. Finally, the fragment *E12* containing the A72T and V91S mutations was obtained. Then *E12* was ligated into the expression vector pPIC3.5 K at the *BamH*I and *Not*I restriction sites to generate the expression plasmid pPIC3.5K-E12. Accordingly, the plasmid pPIC3.5K-E12 was used as a template, and the two individual fragments were amplified using primers P1−1-F/I368T-R and I368T-F/P1−1-R, respectively, and fused by overlap extension PCR to obtain *E13*. Then the *E13* was digested and ligated into pPIC3.5 K, so as to obtain the expression plasmid pPIC3.5K-E13 by the same methods mentioned above. For the construction of *E14,* the plasmid pPIC3.5K-LXYL-P1−1 was used as a template, and the three separate fragments were amplified using primers S3P-F/S69A-A72T-R, S69A-A72T-F/Q192L-R and Q192L-F/P1 − 1-R, respectively. Afterwards, these fragments were fused by the overlap extension PCR to gain *E14*. For the construction of *E15,* the plasmid pPIC3.5K-E4 was used as a template, and the three individual fragments were amplified using primers S3P-F/S69A-A72T-R, S69A-A72T-F/Q192L-R, Q192L-F/S310A-G318A-R and S310A-G318A-F/P1−1-R, respectively, and the four independent fragments were fused by overlap extension PCR to gain *E15*. Accordingly, *E14* and *E15* were digested and ligated into pPIC3.5 K to obtain the expression plasmids pPIC3.5K-E14 and pPIC3.5K-E15, respectively. For constructing the multiple site-directed mutations in E16, the plasmid pPIC3.5K-E15 was used as a template, and the three fragments were amplified using primers S3P-F/S310A-G318A-E322K-R, E322K-T327A-F/I368T-R and I368T-F/P1−1-R, respectively. The three fragments were fused by overlap extension PCR to gain *E16.* Consistently, *E17* was constructed in the same way using with the primers S3P-F/S310A-G318A-E322K-R, E322K-T327A-T334A-F/I368T-R and I368T-F/P1−1-R, respectively. Finally, *E16* and *E17* were digested and ligated into pPIC3.5 K to obtain the expression plasmids pPIC3.5K-

Table 1 List of strains and plasmids used in this study.

Strain or plasmid	Description	Source
Srain		
GS115	Mut$^+$, His$^-$	Invitrogen
GS115-3.5K-P1−1	GS115 integrated with pPIC3.5K-LXYL-P1−1, Mut$^+$, His$^+$, Geneticin^R	Ref. 12
GS115-3.5K-P1−2	GS115 integrated with pPIC3.5K-LXYL-P1−2, Mut$^+$, His$^+$, Geneticin^R	Ref. 12
GS115-P1E1∼E17	GS115 integrated with pPIC3.5K-E1∼E17, Mut$^+$, His$^+$, Geneticin^R	This study
GS115-P1E12-1	GS115-P1E12 integrated with pPICZA-*pdi*, Mut$^+$, His$^+$, Geneticin^R, Zeocin^R	This study
GS115-P1E12-2	GS115-P1E12 integrated with pGAPZA-*pdi*, Mut$^+$, His$^+$, Geneticin^R, Zeocin^R	This study
GS115-P1E12-3	GS115-P1E12 integrated with pPICZA-*vhb*, Mut$^+$, His$^+$, Geneticin^R, Zeocin^R	This study
GS115-P1E12-4	GS115-P1E12 integrated with pGAPZA-*vhb*, Mut$^+$, His$^+$, Geneticin^R, Zeocin^R	This study
GS115-P1E12-5	GS115-P1E12 integrated with pPICZA-*upc*, Mut$^+$, His$^+$, Geneticin^R, Zeocin^R	This study
GS115-P1E12-6	GS115-P1E12 integrated with pGAPZA-*upc*, Mut$^+$, His$^+$, Geneticin^R, Zeocin^R	This study
GS115-P1E12-7	GS115-P1E12 integrated with pPICZA-*vhb* and pPIC6A-*pdi*, Mut$^+$, His$^+$, Geneticin^R, Zeocin^R, Blasticidin^R	This study
GS115-P1E12-8	GS115-P1E12 integrated with pGAPZA-vhb and pPIC6A-pdi, Mut$^+$, His$^+$, Geneticin^R, Zeocin^R, Blasticidin^R	This study
GS115-P1E12-9	GS115-P1E12 integrated with pGAPZA-pdi and pPIC6A-vhb, Mut$^+$, His$^+$, Geneticin^R, Zeocin^R, Blasticidin^R	This study
Plasmid		
pPIC3.5 K	P_{AOX1}, T_{AOX1}, *pBR322 ori*, His4, Amp^R, Geneticin^R	Invitrogen
pPICZA	P_{AOX1}, T_{AOX1}, p*UC ori*, Zeocin^R	Invitrogen
pGAPZA	P_{GAP}, T_{AOX1}, p*UC ori*, Zeocin^R	Invitrogen
pPIC6A	P_{AOX1}, T_{AOX1}, p*UC ori*, Blasticidin^R	Invitrogen
pPIC3.5K-LXYL-P1−1	pPIC3.5 K with *Lxyl-p1−1*, Geneticin^R, His$^+$	Ref. 12
pPIC3.5K-LXYL-P1−2	pPIC3.5 K with *Lxyl-p1−2*, Geneticin^R, His$^+$	Ref. 12
pPIC3.5K-E1-E17	pPIC3.5 K with *E1-E17* mutated from *Lxyl-p1−1*, Geneticin^R, His$^+$	This study
pPICZA-*pdi*	pPICZA with *pdi* (P_{AOX1}), Zeocin^R	This study
pPICZA-*vhb*	pPICZA with *vhb* (P_{AOX1}), Zeocin^R	This study
pPICZA-*upc*	pPICZA with *upc* (P_{AOX1}), Zeocin^R	This study
pGAPZA-*pdi*	pGAPZA with *pdi* (P_{GAP}), Zeocin^R	This study
pGAPZA-*vhb*	pGAPZA with *vhb* (P_{GAP}), Zeocin^R	This study
pGAPZA-*upc*	pGAPZA with *upc* (P_{GAP}), Zeocin^R	This study
pPIC6A-*pdi*	pPIC6A with *pdi* (P_{AOX1}), Blasticidin^R	This study
pPIC6A-*vhb*	pPIC6A with *vhb* (P_{AOX1}), Blasticidin^R	This study

E16 and pPIC3.5K-E17, respectively. Eventually, all the recombinant plasmids with multiple site-directed mutations were confirmed by nucleotide sequence analysis.

2.3. *Expression of LXYL-P1−1 variants in P. pastoris*

The engineered *P. pastoris* strains containing *Lxyl-p1−1* variants were constructed as mentioned previously. Briefly, 10 μg recombinant vectors pPIC3.5K-E1–E17 were linearized with *Sac*I and then introduced into *P. pastoris* GS115 *via* electroporation transformation according to the manufacturer's instructions (Invitrogen, USA). The transformants were initially selected on MD plates (containing 13.4 g/L yeast nitrogen base, 0.4 mg/L biotin, 20 g/L dextrose, and 15 g/L agar) and then were screened for recombinants with multiple gene integration on YPD plates (containing 10 g/L yeast extract, 20 g/L tryptone, 20 g/L D-glucose, and 15 g/L agar) supplemented with 4 mg/mL G418. The recombinant yeasts harboring the *Lxyl-p1−1* variants were firstly inoculated in 500-mL shake flasks containing 100 mL buffered minimal glycerol complex medium (BMGY) medium (containing 10 g/L yeast extract, 20 g/L tryptone, 13.4 g/L YNB, 0.4 mg/L biotin, 10 g/L glycerol, 100 mmol/L potassium phosphate buffer, pH 6.0) at 30 °C with shaking at 200 rpm for 48–60 h. Then methanol was added every day to maintain 1% (*v*/*v*) for the induction of the gene expression. After 7 days of induction, the recombinant enzymes were isolated and purified according to the method described in our previous report[30].

2.4. *β-Xylosidase and β-glucosidase activity analysis of LXYL-P1−1 mutants*

The β-xylosidase and β-glucosidase activities of the purified LXYL-P1−1mutants were measured by detecting the amount of *p*-nitrophenol released from the substrate *p*-nitrophenyl-β-D-xylopyranoside (PNP-Xyl) or *p*-nitrophenyl-β-D-glucopyranoside (PNP-Glc) under the optimum reaction conditions[12]. Concretely, the 60 μL reaction volume contained 50 μL of 5 mmol/L PNP-Xyl or PNP-Glc and 10 μL of 0.1 mg/mL enzyme in 50 mmol/L sodium acetate buffer with pH 5.0. The reaction was performed under 50 °C for 20 min. Reactions were terminated by adding 1 mL saturated $Na_2B_4O_7$ solution. The enzymatic activity was assayed using spectrophotometry based on the absorbance at 405 nm[12]. One unit of activity was defined as the amount of enzyme that catalyzed the formation of 1 nmol/L *p*-nitrophenol per minute.

2.5. Kinetics of LXYL-P1−1 mutants

The kinetic parameters of the recombinant LXYL-P1−1 mutant enzymes against XDT were determined at the XDT concentration ranging from 0.039–5.0 mmol/L as described previously[12]. DT formation was analyzed through HPLC. The kinetic data on XDT were processed by a proportional weighted fit using a nonlinear regression analysis program based on Michaelis–Menten enzyme kinetics. All data were presented as means ± SD of three independent repeats.

2.6. Homology modeling of LXYL-P1−1 three-dimensional structure and molecular docking with XDT

The three-dimensional (3-D) model of LXYL-P1−1 was predicted by Swiss Model Server (http://swissmodel.expasy.org/)[31] using the available structure of the *Aspergillus fumigatus* (Protein Data Bank code 5fji), which has 44% sequence identity and 59% sequence similarity to LXYL-P1−1, as a template. The predicted 3D structure and substrate XDT were selected for the docking experiments with AutoDockTools[32].

2.7. Construction of VHB, PDI and UPC co-expression vectors

All primers used for constructing the co-expression plasmids are shown in Supporting Information Table S2. The *pdi* gene was amplified from the genomic DNA of *P. pastoris* GS115 based on the published sequence using primers PDI-F and PDI-R. The *vhb* gene (GenBank accession number: AF292694) was amplified from the vector pSKVHb[33] using primers VHB-F and VHB-R. The intronless *upc2.1* gene (GenBank accession number: CP020126.1) was amplified from the genomic DNA of *S. cereviase* INVSc1 using primers UPC-F and UPC-R. The purified PCR products were ligated into plasmids pPICZA, pGAPZA and pPIC6A, respectively, and transformed into *E. coli* Top 10 (Transgen, Beijing, China). The transformants were then selected on the low salt LB plates (containing 10 g/L peptone, 5 g/L yeast extract, 5 g/L NaCl, and 15 g/L agar). Eventually, the final recombinant plasmids were validated by DNA sequencing for correct sequence and direction, and were designated as pPICZA-*pdi/vhb/upc*, pGAPZA-*pdi/vhb/upc* and pPIC6A-*pdi/vhb*, respectively.

2.8. Transformation of P. pastoris GS115-P1E12

To construct the engineered strains that co-expressed the molecular chaperone (PDI), *Vitreoscilla* hemoglobin (VHB) and transcriptional factor (UPC) under the control of P_{AOX1} or P_{GAP}, the *Sac* I linearized pPICZA-*pdi*, pGAPZA-*pdi*, pPICZA-*vhb*, pGAPZA-*vhb*, pPICZA-*upc* or pGAPZA-*upc* (10 μg of each plasmid) were respectively transformed into the strain GS115-P1E12 harboring *E12* gene, and the transformants were initially plated on the YPD plates containing 100 μg/mL Zeocin. Then, the multi-copy transformants were screened on the YPD plates containing 1 mg/mL Zeocin. The correct transformants were referred as GS115-P1E12-1, GS115-P1E12-2, GS115-P1E12-3, GS115-P1E12-4, GS115-P1E12-5 and GS115-P1E12-6, respectively. To construct strains that co-expressed the molecular chaperone and the *Vitreoscilla* hemoglobin simultaneously, 10 μg pPIC6A-*pdi* digested with *Avr* II was transformed into GS115-P1E12-3 and GS115-P1E12-4, respectively. The transformants were initially plated on the YPD plates containing 700 μg/mL blasticidin, and the selection was carried out on the YPD plates containing 2 mg/mL blasticidin, which generated the recombinant strains GS115-P1E12-7 and GS115-P1E12-8, respectively. Accordingly, 10 μg pPIC6A-*vhb* digested with *Avr* II was transformed into GS115-P1E12-2 to generate the recombinant strains GS115-P1E12-9.

2.9. Measurement of β-xylosidase activities of the engineered strains

The engineered yeasts GS115-P1E12-1–9 were further inoculated into the 500-mL shake flasks containing 100 mL BMGY medium. The flasks were incubated at 30 °C and 220 rpm for 48–60 h, and then methanol was added every day to maintain 1% (*v/v*) for inducing gene expression during the induction period. Meanwhile, the *β*-xylosidase activity was analyzed based on periodic sampling. The samples were washed twice with dH_2O *via* centrifugation, and the cell pellet was resuspended with dH_2O in the same volume of culture broth. 10 μL cell suspension was added to 100 μL of 5 mmol/L PNP-Xyl, and incubated for 20 min at 50 °C for the catalytic activity analysis. The *β*-xylosidase activity was then evaluated by calculating both U/L (volumetric enzyme activity) and U/g (biomass enzyme activity) as described previously[34].

2.10. Western blotting

The freeze-dried recombinant yeast cells (10 mg) were mixed with 500 μL Yeast Active Protein Extraction buffer (Sangon Biotech Co., Ltd., Shanghai, China) containing phenylmethanesulfonyl fluoride (PMSF) and proteinase inhibitor cocktail, and the mixture was incubated at room temperature for 20 min. Then, the lysed solution was centrifuged for 15 min at 15,000 × *g*, and the supernatant was collected. To quantify the protein concentration, Bradford dye (Bio-rad, CA, USA) was used according to the manufacturer's instructions. To remove the carbohydrates from the enzyme, 45 μL of the supernatant was mixed with 5 μL of 10 × denatured glycoprotein buffer and boiled at 100 °C for 10 min. 5.5 μL of 10 × G5 buffer and 2 μL Endo Hf enzyme (NEB, Ipswitch, MA, USA) were added and incubated at 37 °C for 1 h. Finally, aliquots (10 μg for total protein) of cell lysates were separated on 12% SDS-PAGE, and then transferred onto the PVDF membrane at 200 mA for 100 min. Exposed protein binding sites on the membranes were blocked by incubation in 5% skim milk-Tris-buffered saline (TBS) for 1 h at room temperature. Then, the membranes were further incubated with His-tag mouse monoclonal antibody (1:1000, Applygen Technologies Inc., Beijing, China) at 4 °C overnight. The membranes were then washed with TBST (TBS with 0.05% tween-20) for four times, and incubated with peroxidase-conjugated goat anti-mouse IgG (1:5,000, Applygen Technologies Inc., Beijing, China) for 2 h at room temperature. Afterwards, the membranes were washed with TBST for another four times, and the protein bands were detected using eECL Western blot kit (Cwbiotec, Beijing, China) following the manufacturer's instructions. Finally, the protein bands on SDS-PAGE gels were quantified with arbitrary unit using Quantity One software version 4.5.0 (Bio-Rad).

3. Results

3.1. *Combining the mutated amino acids from low-active LXYL-P1−1 to the high-active LXYL-P1−2*

The 11 aforementioned sites in LXYL-P1−1 (template) were subjected to site-directed mutations in a single or combined manner towards their counterparts in LXYL-P1−2 (Fig. 1). The precise site-directed mutations were shown as follows, $Ser^{3} \rightarrow Pro$, $Ser^{69} \rightarrow Ala$, $Ala^{72} \rightarrow Thr$, $Val^{91} \rightarrow Ser$, $Gln^{192} \rightarrow Leu$, $Ser^{310} \rightarrow Ala$, $Gly^{318} \rightarrow Ala$, $Glu^{322} \rightarrow Lys$, $Glu^{327} \rightarrow Ala$, $Thr^{334} \rightarrow Ala$, and $Ile^{368} \rightarrow Thr$. Thus, the variants E1 to E17 were generated (Fig. 2).

Moreover, the activities of the purified enzymes were measured through hydrolysis of the chromogenic substrates PNP-Xyl and PNP-Glu, respectively[30]. As shown in Fig. 2 and Supporting Information Table S3, apart from E1 (S3P), E5 (Q192L), E6 (E310A) and E7 (E318A), all other single site-directed mutants (variants), including E2 (S69A), E3 (A72T), E4 (V91S), E8 (E322K), E9 (E327A), E10 (T334A) and E11 (I368T), had displayed higher activities of β-xylosidase and β-glucosidase than those of LXYL-P1−1, in which E3 (A72T) showed similar β-D-xylosidase activity but higher β-D-glucosidase activity compared with those of E2 (S69A). These finding suggested the presence of upward bias in their activities after mutation. Moreover, the β-glucosidase activities of E3, E4 and E11, as well as the β-xylosidase activity of E11 even surpassed those of LXYL-P1−2. Subsequently, E3 (A72T) and E4 (V91S) were selected to construct the double mutant E12 (A72T/V91S). Later, the triple mutant E13 (A72T/V91S/I368T) was constructed by combining E12 with E11 (I368T, which came up with LXYL-P1−2 in terms of β-xylosidase and β-glucosidase activities). As shown in Fig. 2 and Supporting Information Table S3, the β-xylosidase and β-glucosidase activities of the double mutant E12 (A72T/V91S) were markedly improved (14.10 ± 1.33 and 35.94 ± 0.63 U/mg $\times 10^4$, respectively), which were 5.7 and 7.2 times as high as those of LXYL-P1−1 (2.46 ± 0.27 and 4.97 ± 0.09 U/mg $\times 10^4$, respectively) and even 2.8- and 3-folds higher than those of LXYL-P1−2 (5.03 ± 0.14 and 12.05 ± 0.49 U/mg $\times 10^4$, respectively). However, no further increase in the enzyme activity was observed in the triple mutant E13 (A72T/V91S/I368T) (2.35 ± 0.22 and 8.19 ± 0.69 U/mg $\times 10^4$, respectively) compared with those of E12. To investigate whether these mutations had positive synergistic effects, the quadruple mutation (E14), septuple mutation (E15), decuple mutation (E16), as well as the hendecuple mutation (E17) were constructed, respectively, in which E17 contained all of the eleven aforementioned mutation sites. Unfortunately, the activities of these 4 mutants were shown to be lower than those of LXYL-P1−2, except that the β-xylosidase activity of E16 and the β-glucosidase activity of E17 were 61% and 66% higher than those of LXYL-P1−1, respectively (Fig. 2 and Supporting Information Table S3).

3.2. *Kinetic analysis of the mutated enzymes against XDT*

The β-xylosidase catalytic efficiencies (k_{cat}/K_m: $[s^{-1} \cdot (mmol/L)^{-1}]$) against substrate XDT were evaluated in the double mutant E12, as well as the single mutants E3 and E4, respectively. As summarized in Table 2, the K_m values of LXYL-P1−1 and

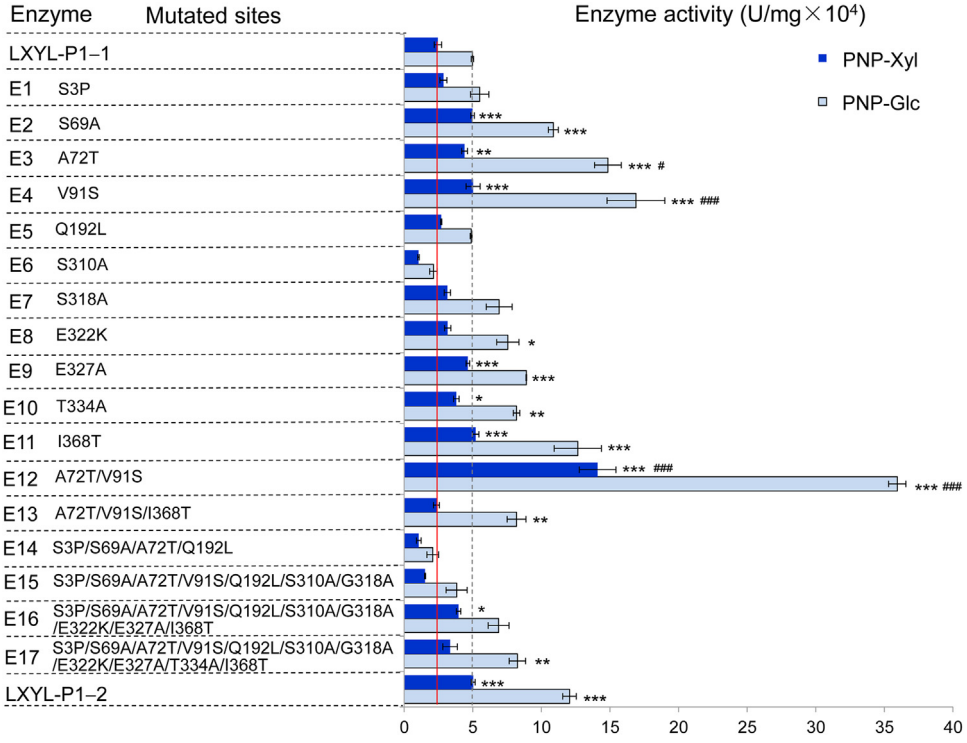

Figure 2 Specific activities of LXYL-P1−1-derived mutants against PNP-Xyl and PNP-Glc. Data are mean ± SD. $n=3$, $^{*}P<0.05$ *vs* LXYL-P1−1, $^{**}P<0.01$ *vs* LXYL-P1−1, $^{***}P<0.001$ *vs* LXYL-P1−1; $P<0.05$ *vs* LXYL-P1−2, $P<0.01$ *vs* LXYL-P1−2, $P<0.001$ *vs* LXYL-P1−2.

LXYL-P1−2 (controls) were similar, but the substrate turnover value (k_{cat}, calculated from V_{max}) of LXYL-P1−2 was 2.3 times as high as that of LXYL-P1−1. As a result, the catalytic efficiency of LXYL-P1−2 was 2.6 times higher than that of LXYL-P1−1. The affinity of E3 (A72T) towards XDT was apparently lower than those of the two controls, but its turnover value (5.35 s^{-1}) had surpassed that of LXYL-P1−1 (2.13 s^{-1}) by 2.5 times and was even higher than that of LXYL-P1−2 (4.89 s^{-1}). Therefore, E3 had displayed higher catalytic efficiency relative to that of LXYL-P1−1 (4.54 *vs.* 3.72 [$s^{-1} \cdot (mmol/L)^{-1}$]). Similarly, the V91S mutation in E4 resulted in a 1.7-fold increase in the catalytic efficiency (6.26 *vs.* 3.72 [s^{-1} $(mmol/L)^{-1}$]), which could be ascribed to the apparent increase in the k_{cat} and the minor increase in the K_m. Typically, E12 had exhibited the highest substrate affinity (depicted as the lowest K_m value: 0.30 mmol/L), which had surpassed those of LXYL-P1−1 (K_m: 0.57 mmol/L) and LXYL-P1−2 (K_m: 0.51 mmol/L), but its k_{cat} value was between those of LXYL-P1−1 and LXYL-P1−2, thus endowing it with the highest catalytic efficiency (11.23 [s^{-1} $(mmol/L)^{-1}$]) among the three mutants and the native controls.

3.3. Substrate–enzyme docking analysis

GH3 β-glucosidase from *Aspergillus fumigatus* (Protein Data Bank code 5fji) had displayed the highest sequence identity (44%) and sequence similarity (59%) to those of LXYL-P1−1. As a result, it was selected as the template for the homology modeling of the LXYL-P1−1 structure. Typically, the sequence alignment between LXYL-P1−1 and the template was shown in Fig. 3A. Moreover, the three-dimensional structure of LXYL-P1−1 was predicted using molecular modeling (http://swissmodel.Expasy.org/). According to Fig. 3B and C, LXYL-P1−1 possessed a triosephosphate isomerase (TIM) barrel-like domain at N-terminus, which was in accordance with that of LXYL-P1−2, as predicted previously[30]. In addition, it was found that, the 10 aforementioned amino acids (Ser^3 was missing from the modeling), which had different properties to those of LXYL-P1−2 were almost located within the N-terminus of the TIM barrel-like domain. Among them, Ser^{69}, Ala^{72}, Val^{91}, Gln^{192}, Glu^{322}, Glu^{327}, Thr^{334} and Ile^{368} were located on the surface of the predicted structure, while Ser^{310} and Gly^{318} were situated within the structure. In addition, Val^{91}, Ser^{310}, Gly^{318}, Glu^{322} and Glu^{327} were close to the catalytic nucleophile Asp^{300} [12, 35].

To further explore the potential molecular mechanism of the improved catalytic property of E12 (A72T/V91S), the molecular docking between the enzyme and the substrate XDT was conducted based on the homology modeling. Fig. 4A and B suggested that, residue Ala^{72} was located on the LXYL-P1−1 surface, and A72T mutation in mutant E12 might lead to conformational change in the loop near XDT, which might positively influence the entrance of XDT. However, residue Val^{91} was close to the nucleophile Asp^{300}, which was located near the XDT entrance path to the active pocket. Only two internal hydrogen bonds were found between Val^{91} and the surrounding amino acid residues in LXYL-P1−1, which were Gln^{108} and Trp^{301}. By contrast, four hydrogen bonds were formed among Ser^{91}, Gln^{108}, Trp^{301} and substrate XDT in variant E12, which could enhance the enzyme-substrate interaction (Fig. 4C and D). Thus, among the microenvironment of the LXYL-P1−1 structure, the combination of A72T and V91S might positively promote the enzyme-XDT interaction through enhancing the hydrogen bonds and altering the loop conformation. Eventually this would result in the remarkably increased substrate affinity and higher catalytic efficiency (Table 2).

3.4. Engineering yeast for improved β-glycosidase production

The recombinant yeast GS115-3.5K-P1–2 that produced LXYL-P1−2 had been applied for the high-cell-density fermentation and for the biocatalysis of XDT[36,37]. Specifically, E12 obtained in this study had displayed the highest β-xylosidase and β-glucosidase activities. Therefore, the recombinant yeast GS115-P1E12 harboring *E12* gene would be an ideal candidate to replace GS115-P1−2 for industrial application. To further up-regulate E12 expression, the genes of molecular chaperone (*pdi*), *Vitreoscilla* hemoglobin (*vhb*) or transcriptional factor (*upc*), under the control of P_{AOX1} or P_{GAP}, was introduced into GS115-P1E12, respectively, generating the following recombinant strains: GS115-P1E12-1 (co-expressing *pdi* controlled by P_{AOX1}), GS115-P1E12-2 (co-expressing *pdi* controlled by P_{GAP}), GS115-P1E12-3 (co-expressing *vhb* controlled by P_{AOX1}), GS115-P1E12-4 (co-expressing *vhb* controlled by P_{GAP}), GS115-P1E12-5 (co-expressing *upc* controlled by P_{AOX1}), and GS115-P1E12-6 (co-expressing *upc* controlled by P_{GAP}). Subsequently, the resultant strains (Fig. 5A) were further cultivated for 7 days prior to the determination of the volumetric and biomass enzyme (β-xylosidase) activities described

Table 2 Kinetic parameters for the mutated enzymes using XDT as the substrate.

Parameter	LXYL-P1−1	LXYL-P1−2	E3	E4	E12
V_{max} (μmol/L min)	3.55 (±0.08)	8.16 (±0.15)***	8.92 (±0.85)***	7.93 (±0.59)***	5.54 (±0.29)***
K_m (mmol/L)	0.57 (±0.02)	0.51 (±0.01)	1.18 (±0.13)***	0.76 (±0.09)*	0.30 (±0.03)**
k_{cat} (s^{-1})	2.13 (±0.05)	4.89 (±0.09)***	5.35 (±0.51)***	4.75 (±0.35)***	3.32 (±0.17)***
k_{cat}/K_m [$s^{-1} \cdot$ $(mmol/L)^{-1}$]	3.72 (±0.06)	9.67 (±0.10)***	4.54 (±0.04)**	6.26 (±0.30)***	11.23 (±0.56)***

Note: Data are mean (±SD). $n = 3$,
*$P < 0.05$ *vs* LXYL-P1−1.
**$P < 0.01$ *vs* LXYL-P1−1.
***$P < 0.001$ *vs* LXYL-P1−1.

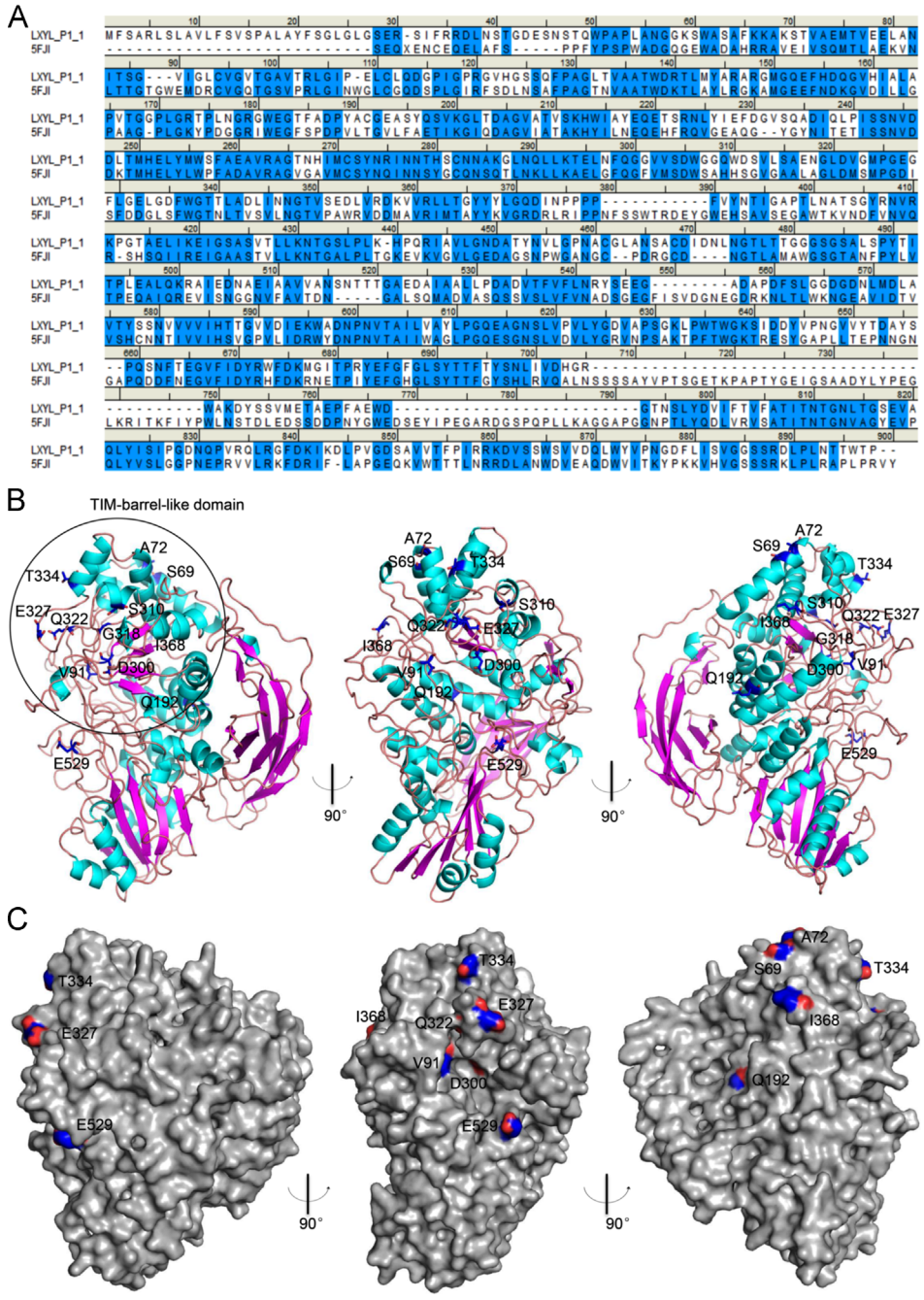

Figure 3 The homology model of LXYL-P1−1 predicted based on the template GH3 β-glucosidase from *Aspergillus fumigatus* (PDB ID: 5fji) using the Swiss Model. (A) Sequence alignment between LXYL-P1−1 and the template GH3 β-glucosidase from *Aspergillus fumigatus* (PDB ID: 5fji). Identical and similar residues are highlighted in blue. (B) Three-dimensional structure view of LXYL-P1−1. α-Helices are shown in cyan, β-strands are in magentas and loops are in salmon. (C) Surface view of LXYL-P1−1. The catalytic sites (Asp^{300} and Glu^{529}) and the amino acids different from those of LXYL-P1−2 in properties are indicated in blue.

previously[30]. The results indicated that, except for UPC, both PDI and VHB could apparently enhance the volumetric and biomass enzyme activities compared with those of control; typically, VHB had exerted the highest effect on day 7 (Figs. 5 and 7). Additionally, the two promoters (P_{AOX1} and P_{GAP}) showed similar effects on driving the expression of both *pdi* and *vhb*, in which P_{AOX1} had exerted a slightly higher effect on improving the biomass enzyme activities (Fig. 5).

To examine the synergetic effect, both *pdi* and *vhb* genes were co-expressed in GS115-P1E12 host, under different combinations of P_{AOX1} and P_{GAP} (Fig. 6A), and three recombinant strains were generated, including GS115-P1E12-7, GS115-P1E12-8 and

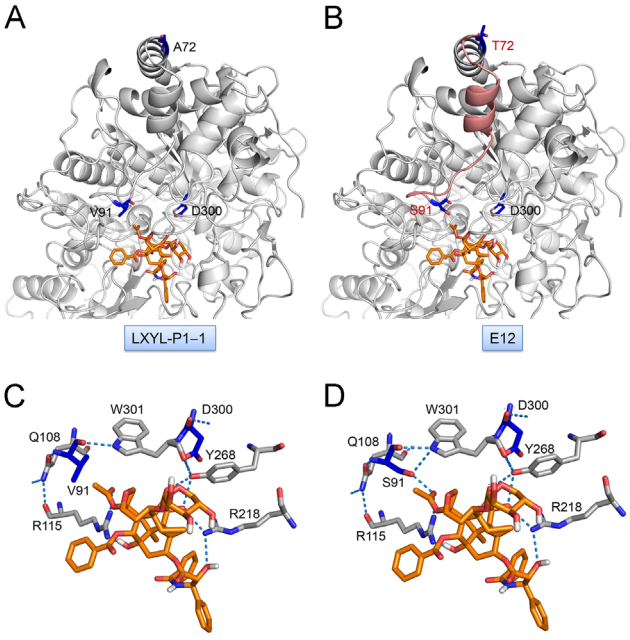

Figure 4 Partial view of enzyme-XDT docking. (A) Side view of LXYL-P1−1 with XDT, showing Ala^{72}, and Val^{91}. (B) Side view of E12 with XDT, in which Ala^{72} and Val^{91} are replaced by Thr^{72} and Ser^{91}, respectively. The loops near the active pocket are indicated in salmon. (C) Hydrogen bonds formed between Val^{91} and surrounding amino acid residues. (D) Hydrogen bonds formed between Ser^{91} and surrounding amino acid residues or substrate. Hydrogen bonds are shown as dotted lines. The carbon atoms of XDT are shown in orange. The nucleophile Asp^{300} (catalytic site), Ala^{72}/Thr^{72}, and Val^{91}/Ser^{91} are colored in blue.

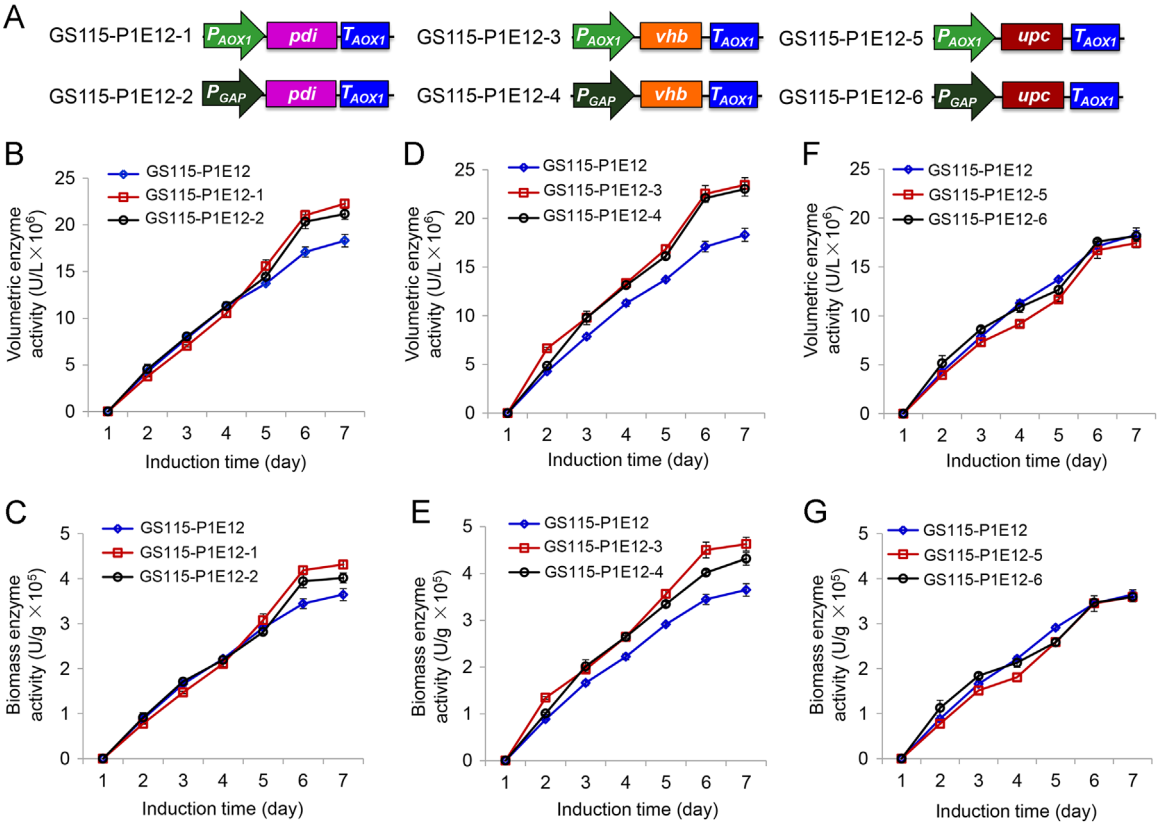

Figure 5 Effects of PDI, VHB and UPC on β-xylosidase (E12) expression. (A) Strains with different plasmids for over-expression of *pdi*, *vhb* and *upc*. (B, D and F) Volumetric enzyme activities. (C, E and G) Biomass enzyme activities. Data are mean ± SD. $n = 3$.

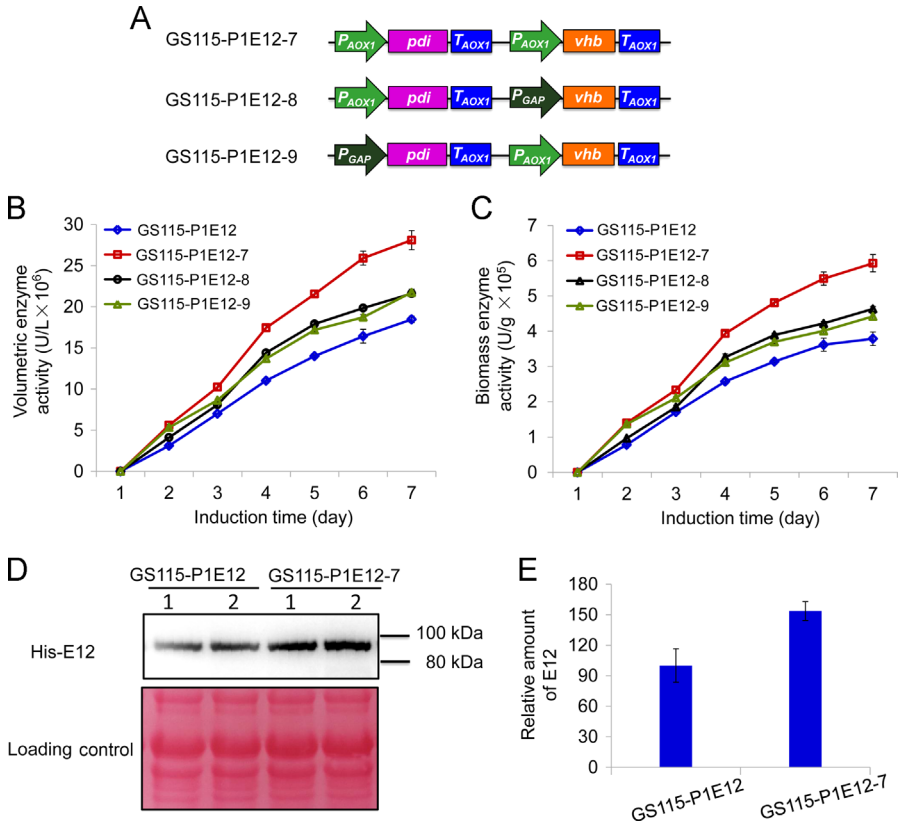

Figure 6 Synergetic effect of PDI and VHB on β-xylosidase (E12) expression. (A) Strains with different plasmids for over-expression of *pdi* and *vhb*. (B) Volumetric enzyme activities. (C) Biomass enzyme activities. (D) Western blot analysis of de-glycosylated E12 from GS115-P1E12 and GS115-P1E12-7 using anti-His antibody. The Ponceau-*S*-stained blot (below) is the loading control[41]. (E) Relative protein amount of each sample quantified with Quantity One Software. The values are indicated as mean ± SD ($n = 3$) of independent assays.

GS115-P1E12-9. After 7 days of cultivation, all these three strains had surpassed the control (GS115-P1E12) in terms of both volumetric and biomass enzyme activities (Fig. 6B and C). Among them, GS115-P1E12-7 had exhibited the highest volumetric (28.10×10^6 U/L) and biomass (5.93×10^5 U/g) enzyme activities, which had amounted to 52.85% and 59.50% higher than those of the control strain GS115-P1E12 (Fig. 7). Western blotting data indicated that E12 expression was up-regulated by approximately 50% in GS115-P1E12-7 compared with that in the control (Fig. 6D and E), which was consistent with the improved volumetric and biomass enzyme activities. Additionally, as summarized in Fig. 7, the biomass enzyme activity of GS115-P1E12-7 was about 7.5 times as high as that of GS115-3.5K-P1−1, while 4 times as high as that of GS115-3.5K-P1−2.

4. Discussions

The glycosidase activity of LXYL-P1−2 was markedly higher than that of LXYL-P1−1, but the sequence difference between the two enzymes was only less than 3%. Moreover, of the 21 different amino acids, only 11 had exhibited significant differences in terms of their polarity and acidic-basic properties (Fig. 1). Site-directed mutations of these 11 amino acids from the low-active LXYL-P1−1 to the high-active LXYL-P1−2 were carried out, and a total of 17 variants were obtained, in which E16 and E17 had harbored 10 and 11 mutated amino acids, respectively (Fig. 2).

Our results showed that Ala^{69}, Thr^{72}, Ser^{91}, Lys^{322}, Ala^{327}, Ala^{334} and Thr^{368} exhibited the upward bias in their activities, with Thr^{72}, Ser^{91}, and Thr^{368} being the top three amino acids. Besides, different combinations of mutations from 2 to 11 sites were made, in which the double mutant E12 (A72T/V91S) displayed the highest enzyme activities. Specifically, it had even surpassed LXYL-P1−2 by 2.8- and 3-fold with regard to β-xylosidase and β-glucosidase activities, respectively. Consequently, the catalytic efficiency of E12 against XDT was apparently increased compared with that of LXYL-P1−2 due to an increased substrate affinity (Table 2). However, other combinations of mutations would not lead to improved activities compared with those of LXYL-P1−2; alternatively, they would even result in decreased activities compared with those of LXYL-P1−1 (E14, E15) (Fig. 2). Furthermore, E16 and E17, which contained 10 and 11 aforementioned mutations, respectively, shared the highest similarity to LXYL-P1−2 in terms of polarity and acidic-basic properties (Fig. 1). Nonetheless, the enzyme specific activities of these two variants were still lower than those of LXYL-P1−2, even though they had surpassed those of LXYL-P1−1 (Fig. 2). Such finding suggests that other amino acids, including Phe^{105}, Leu^{155}, Asp^{223}, Ile^{224}, Ser^{278}, Pro^{309} Val^{337}, Glu^{338} Val^{337}, Glu^{338}, Ala^{354}, and Ile^{357} among the 21 different amino acids in LXYL-P1−2 may also contribute to the positive effects on enzyme activity. It can be concluded from these results that, firstly, the combination of the 21 different amino acids in LXYL-P1−2 is not the best one, since the 19 amino acids of E12 (with the highest activity) in this study are

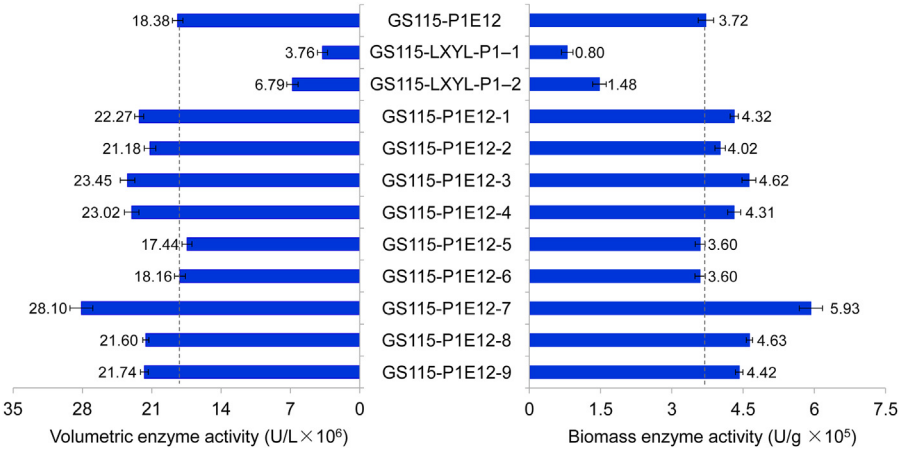

Figure 7 Comparison of different strains on volumetric and biomass enzyme activities after cultivation for 7 days. Data are mean ± SD. $n = 3$.

of LXYL-P1−1 origin, while only 2 amino acids are the same as those in LXYL-P1−2. Secondly, the biocatalytic property is determined by the conformational fitness to the substrate, which is the outcome of interactions among various amino acids in the whole enzyme.

Molecular docking results showed that in the microenvironment of LXYL-P1−1 structure, the combinatorial mutation of A72T and V91S might positively promote the enzyme-XDT interaction. This was achieved through increasing the hydrogen bonds among Ser^{91} and other surrounding amino acids as well as XDT, apart from altering the loop conformation near XDT (Fig. 4). This might partially explain the reason why the mutant E12 (A72T/V91S) had exhibited apparently higher activity.

To further promote E12 production by the recombinant cells of GS115-P1E12, the chaperone protein PDI, bacterial *Vitreoscilla* hemoglobin VHB, and transcription factor UPC, were co-expressed with E12 in the yeast host GS115-P1E12. The results indicated that except for UPC, both PDI and VHB could up-regulate E12 expression, with VHB exerting a higher effect (Fig. 5). Moreover, both P_{AOX1} and P_{AOX1} could also efficiently drive enzyme production. Subsequently, these two helper factors were co-expressed with E12 and driven by different promoter combinations. Notably, the best results were observed when the two genes were controlled by P_{AOX1} (Fig. 6). The volumetric and biomass activities of all variants obtained in this study, together with those of the original GS115-3.5K-P1−1 and GS115-3.5K-P1−2, are summarized in Fig. 7. As shown in Fig. 7, the volumetric and biomass enzyme activities of GS115-P1E12-7 reached 28.1×10^6 U/L and 5.93×10^4 U/g, respectively, which were 4 times higher than those of GS115-3.5K-P1−2 under the same culture conditions. These findings revealed that over-expressing VHB could enhance oxygen supply and efficient oxygen utilization, so as to up-regulate the expression of heterologous protein. Moreover, over-expressing PDI could also promote the correct protein folding and up-regulate the heterologous protein expression. The recombinant yeast GS115-3.5K-P1−2 had been used for the high-cell-density fermentation and catalysis of hydrolyzing xylosyl group from XDT to form DT for the Taxol semi-synthesis[34,36,37]. Therefore, replacing GS115-3.5K-P1−2 with GS115-P1E12-7 should greatly reduce the catalytic cost, which might benefit the industrial application.

5. Conclusion and perspectives

Taken together, site-directed mutations of the 11 different amino acids were carried out from the low-active LXYL-P1−1 to the high-active LXYL-P1−2. The results suggested that, seven amino acids, including Ser^{69}, Thr^{72}, Ser^{91}, Glu^{322}, Glu^{327}, Glu^{334} and Thr^{368}, were the important amino acids with upward bias in their activities. Particularly, A72T and V91S mutations in E3 and E4 had rendered them the superior enzyme activities among all the single-site mutants of LXYL-P1−1. Moreover, the best variant E12 with double mutation (A72T/V91S) was also obtained, which had notably improved the catalytic efficiency compared with that of the original LXYL-P1−1 and even surpassed that of the high-active LXYL-P1−2. The possible mechanism for the improvement was proposed by homology modeling and molecular docking between E12 and 7-*β*-xylosyl-10-deacetyltaxol. Besides, the recombinant yeast GS115-P1E12-7 was also constructed based on variant E12, which harbored the molecular chaperone gene *pdi* (*P. pastoris* origin) and the bacterial hemoglobin gene *vhb* (*Vitreoscilla* origin) driven by the inducible promoter P_{AOX1}. Typically, the volumetric and biomass enzyme activities of the recombinant yeast GS115-P1E12-7 were 4 times higher than those of the GS115-3.5K-P1−2 control. Therefore, GS115-P1E12-7 can be used to replace GS115-3.5K-P1−2 for industrial purpose, which will greatly increase the catalytic efficiency and significantly reduce the cost. In the future, saturated mutagenesis on Ser^{69}, Thr^{72}, Ser^{91} and Thr^{368}, followed by different combinations may be conducted to find more active mutants. Since enzymes with different variants are widely distributed in the nature[38–40], our study may serve as a paradigm for acquiring highly active enzyme variants, which can be used for the drug structural modification or optimization.

Acknowledgments

This work was supported by the National Natural Science Foundation of China (Grants nos. 81573325 and 31270796), the National Mega-project for Innovative Drugs (Grants nos. 2018ZX09711001-006-001 and 2012ZX09301002-001-005, China), the fundamental Research Funds for the Central Universities (Grant no. 2017PT35001, China), and CAMS Innovation

Fund for Medical Sciences (Grant no. CIFMS-2017-I2M-4-004, China).

Appendix A. Supporting information

Supplementary data associated with this article can be found in the online version at https://doi.org/10.1016/j.apsb.2018.11.003.

References

1. Cantarel BL, Coutinho PM, Rancurel C, Bernard T, Lombard V, Henrissat B. The Carbohydrate-Active EnZymes database (CAZy): an expert resource for glycogenomics. *Nucleic Acids Res* 2008;**37**:D233–8.
2. Faure D. The family-3 glycoside hydrolases: from housekeeping functions to host-microbe interactions. *Appl Environ Microbiol* 2002;**68**:1485–90.
3. Vuong TV, Wilson DB. Glycoside hydrolases: catalytic base/nucleophile diversity. *Biotechnol Bioeng* 2010;**107**:195–205.
4. Liu M, Kong JQ. The enzymatic biosynthesis of acylated steroidal glycosides and their cytotoxic activity. *Acta Pharm Sin B* 2018;**6**:981–94.
5. Juturu V, Wu JC. Microbial xylanases: engineering, production and industrial applications. *Biotechnol Adv* 2012;**30**:1219–27.
6. Shao W, Xue Y, Wu A, Kataeva I, Pei J, Wu H, et al. Characterization of a novel β-xylosidase, XylC, from *Thermoanaerobacterium saccharolyticum* JW/SL-YS485. *Appl Environ Microbiol* 2011;**77**:719–26.
7. Teng C, Jia H, Yan Q, Zhou P, Jiang Z. High-level expression of extracellular secretion of a β-xylosidase gene from *Paecilomyces thermophila in Escherichia coli*. *Bioresour Technol* 2011;**102**:1822–30.
8. Rowinsky EK, Donehower RC. Paclitaxel (Taxol). *New Engl J Med* 1995;**332**:1004–14.
9. Wani MC, Taylor HL, Wall ME, Coggon P, McPhail AT. Plant antitumor agents. VI. Isolation and structure of Taxol, a novel antileukemic and antitumor agent from *Taxus brevifolia*. *J Am Chem Soc* 1971;**93**:2325–7.
10. Cragg GM. Paclitaxel (Taxol®): a success story with valuable lessons for natural product drug discovery and development. *Med Res Rev* 1998;**18**:315–31.
11. Liu WC, Gong T, Zhu P. Advances in exploring alternative Taxol sources. *RSC Adv* 2016;**6**:48800–9.
12. Cheng HL, Zhao RY, Chen TJ, Yu WB, Wang F, Cheng KD, et al. Cloning and characterization of the glycoside hydrolases that remove xylosyl groups from 7-β-xylosyl-10-deacetyltaxol and its analogues. *Mol Cell Proteomics* 2013;**12**:2236–48.
13. Li BJ, Wang H, Gong T, Chen JJ, Chen TJ, Yang JL, et al. Improving 10-deacetylbaccatin III-10-β-*O*-acetyltransferase catalytic fitness for Taxol production. *Nat Commun* 2017;**8**:15544.
14. Ahmad M, Hirz M, Pichler H, Schwab H. Protein expression in *Pichia pastoris*: recent achievements and perspectives for heterologous protein production. *Appl Microbiol Biotechnol* 2014;**98**:5301–17.
15. Cos O, Ramón R, Montesinos JL, Valero F. Operational strategies, monitoring and control of heterologous protein production in the methylotrophic yeast *Pichia pastoris* under different promoters: a review. *Microb Cell Fact* 2006;**5**:17.
16. Damasceno LM, Huang CJ, Batt CA. Protein secretion in *Pichia pastoris* and advances in protein production. *Appl Microbiol Biotechnol* 2012;**93**:31–9.
17. Chien LJ, Lee CK. Expression of bacterial hemoglobin in the yeast, *Pichia pastoris*, with a low O_2-induced promoter. *Biotechnol Lett* 2005;**27**:1491–7.
18. Stark BC, Pagilla KR, Dikshit KL. Recent applications of *Vitreoscilla* hemoglobin technology in bioproduct synthesis and bioremediation. *Appl Microbiol Biotechnol* 2015;**99**:1627–36.
19. Zhang L, Li Y, Wang Z, Xia Y, Chen W, Tang K. Recent developments and future prospects of *Vitreoscilla* hemoglobin application in metabolic engineering. *Biotechnol Adv* 2007;**25**:123–36.
20. Feng J, Gu Y, Sun Y, Han LF, Yang C, Zhang W, et al. Metabolic engineering of *Bacillus amyloliquefaciens* for poly-γ-glutamic acid (γ-PGA) overproduction. *Microb Biotechnol* 2014;**7**:446–55.
21. Su Y, Li X, Liu Q, Hou Z, Zhu X, Guo X, et al. Improved poly-γ-glutamic acid production by chromosomal integration of the *Vitreoscilla* hemoglobin gene (*vgb*) in *Bacillus subtilis*. *Bioresour Technol* 2010;**101**:4733–6.
22. Wang X, Sun Y, Shen X, Ke F, Zhao H, Liu Y, et al. Intracellular expression of *Vitreoscilla* hemoglobin improves production of *Yarrowia lipolytica* lipase LIP2 in a recombinant *Pichia pastoris*. *Enzyme Microb Technol* 2012;**50**:22–8.
23. Wu JM, Fu WC. Intracellular co-expression of *Vitreoscilla* hemoglobin enhances cell performance and β-galactosidase production in *Pichia pastoris*. *J Biosci Bioeng* 2012;**113**:332–7.
24. Chen H, Chu J, Zhang S, Zhuang Y, Qian J, Wang Y, et al. Intracellular expression of *Vitreoscilla* hemoglobin improves *S*-adenosylmethionine production in a recombinant *Pichia pastoris*. *Appl Microbiol Biotechnol* 2007;**74**:1205–12.
25. Inan M, Aryasomayajula D, Sinha J, Meagher MM. Enhancement of protein secretion in *Pichia pastoris* by overexpression of protein disulfide isomerase. *Biotechnol Bioeng* 2006;**93**:771–8.
26. Samuel P, Prasanna Vadhana AK, Kamatchi R, Antony A, Meenakshisundaram S. Effect of molecular chaperones on the expression of *Candida antarctica* lipase B in *Pichia pastoris*. *Microbiol Res* 2013;**168**:615–20.
27. Yang H, Tong J, Lee CW, Ha S, Eom SH, Im YJ. Structural mechanism of ergosterol regulation by fungal sterol transcription factor Upc2. *Nat Commun* 2015;**6**:6129.
28. Bryksin AV, Matsumura I. Overlap extension PCR cloning: a simple and reliable way to create recombinant plasmids. *BioTechniques* 2010;**48**:463–5.
29. Heckman KL, Pease LR. Gene splicing and mutagenesis by PCR-driven overlap extension. *Nat Protoc* 2007;**2**:924–32.
30. Chen JJ, Liang X, Li HX, Chen TJ, Zhu P. Improving the catalytic property of the glycoside hydrolase LXYL-P1-2 by directed evolution. *Molecules* 2017;**22**:2133.
31. Schwede T, Kopp J, Guex N, Peitsch MC. SWISS-MODEL: an automated protein homology-modeling server. *Nucleic Acids Res* 2003;**31**:3381–5.
32. Huey R, Morris GM. In: *Using AutoDock 4 with AutoDocktools: a tutorial*. La Jolla, California:: The Scripps Research Institute; 54–6.
33. Shen J, Zheng H, Zhi X, Shi Y, Huang Y, Wang W, et al. Improvement of amorpha-4,11-diene production by a yeast-conform variant of *Vitreoscilla* hemoglobin. *Z Naturforsch C* 2012;**67**:195–207.
34. Yu WB, Liang X, Zhu P. High-cell-density fermentation and pilot-scale biocatalytic studies of an engineered yeast expressing the heterologous glycoside hydrolase of 7-β-xylosyltaxanes. *J Ind Microbiol Biotechnol* 2013;**40**:133–40.
35. Wang F, Zhu P. Prediction and preliminary functional analysis of the potential active center of the glycoside hydrolases LXYL-P1-1 and LXYL-P1-2. *Mycosystema* 2013;**32**:846–54.
36. Liu WC, Gong T, Wang QH, Liang X, Chen JJ, Zhu P. Scaling-up fermentation of *Pichia pastoris* to demonstration-scale using new methanol-feeding strategy and increased air pressure instead of pure oxygen supplement. *Sci Rep* 2016;**6**:18439.
37. Liu WC, Zhu P. Pilot studies on scale-up biocatalysis of 7-β-xylosyl-10-deacetyltaxol and its analogues by an engineered yeast. *J Ind Microbiol Biotechnol* 2015;**42**:867–76.
38. Juhász T, Szengyel Z, Réczey K, Siika-Aho M, Viikari L. Characterization of cellulases and hemicellulases produced by *Trichoderma reesei* on various carbon sources. *Process Biochem* 2005;**40**:3519–25.
39. Tsukada T, Igarashi K, Yoshida M, Samejima M. Molecular cloning and characterization of two intracellular β-glucosidases belonging to glycoside hydrolase family 1 from the basidiomycete *Phanerochaete chrysosporium*. *Appl Microbiol Biotechnol* 2006;**73**:807–14.

40. Wang TY, Chen HL, Lu MY, Chen YC, Sung HM, Mao CT, et al. Functional characterization of cellulases identified from the cow rumen fungus *Neocallimastix patriciarum* W5 by transcriptomic and secretomic analyses. *Biotechnol Biofuels* 2011;**4**:24.

41. Romero-Calvo I, Ocón B, Martínez-Moya P, Suárez MD, Zarzuelo A, Martínez-Augustin O, et al. Reversible Ponceau staining as a loading control alternative to actin in Western blots. *Anal Biochem* 2010;**401**:318–20.